

Effects of visual stimulation on LFPs, spikes, and LFP-spike relations in PRR

Eun Jung Hwang and Richard A. Andersen

Division of Biology, California Institute of Technology, Pasadena, California

Submitted 20 September 2010; accepted in final form 6 February 2011

Hwang EJ, Andersen RA. Effects of visual stimulation on LFPs, spikes, and LFP-spike relations in PRR. *J Neurophysiol* 105: 1850–1860, 2011. First published February 9, 2011; doi:10.1152/jn.00802.2010.—Local field potentials (LFPs) have shown diverse relations to the spikes across different brain areas and stimulus features, suggesting that LFP-spike relationships are highly specific to the underlying connectivity of a local network. If so, the LFP-spike relationship may vary even within one brain area under the same task condition if neurons have heterogeneous connectivity with the active input sources during the task. Here, we tested this hypothesis in the parietal reach region (PRR), which includes two distinct classes of motor goal planning neurons with different connectivity to the visual input, i.e., visuomotor neurons receive stronger visual input than motor neurons. We predicted that the visual stimulation would render both the spike response and the LFP-spike relationship different between the two neuronal subpopulations. Thus we examined how visual stimulations affect spikes, LFPs, and LFP-spike relationships in PRR by comparing their planning (delay) period activity between two conditions: with or without a visual stimulus at the reach target. Neurons were classified as visuomotor if the visual stimulation increased their firing rate, or as motor otherwise. We found that the visual stimulation increased LFP power in gamma bands >40 Hz for both classes. Moreover, confirming our prediction, the correlation between the LFP gamma power and the firing rate became higher for the visuomotor than motor neurons in the presence of visual stimulation. We conclude that LFPs vary with the stimulation condition and that the LFP-spike relationship depends on a given neuron's connectivity to the dominant input sources in a particular stimulation condition.

local field potential-spike correlation; parietal reach region; gamma band; visuomotor and motor neurons; parietal cortex; bottom-up and top-down input; reaches

A NUMBER OF STUDIES REPORTED that local field potentials (LFPs) encode information that was previously shown to modulate the spiking activity in the same brain region. For example, LFPs in the primary visual cortex encode visual features such as stimulus orientation and contrast (Gray and Singer 1989; Henrie and Shapley 2005). LFPs in area MT are tuned to the speed and direction of moving visual stimuli (Liu and Newsome 2006). LFPs in the posterior parietal cortex are modulated by the grasp type in the anterior intraparietal area (Asher et al. 2007), the saccade goal in the lateral intraparietal area (Pesaran et al. 2002), and the reach goal in the parietal reach region (PRR) (Scherberger et al. 2005). In the primary motor cortex, LFPs systematically vary with the hand movement direction, velocity, and grasp type (Rickert et al. 2005; Heldman et al. 2006; Spinks et al. 2008). In general, however, LFPs show less

sensitivity to changes in these variable features (Pesaran et al. 2002; Scherberger et al. 2005; Asher et al. 2007) and to changes in recording location than spikes in the same region (Axel and Reinhard 2000; Leopold and Logothetis 2003; O'Leary and Hatsopoulos 2006; Berens et al. 2008).

The different sensitivity to changes both in the feature space (tuning) and cortical space between LFPs and spikes may be related to their distinct signal origins. LFPs seem to reflect the average membrane potentials of nearby neurons while spikes are the output of nonlinear transformations of the membrane potentials (e.g., threshold and saturation) by individual neurons, as indicated by the following evidence. First, LFPs are extremely similar to subthreshold membrane potentials of nearby neurons (Penttonen et al. 1998; Poulet and Petersen 2008) and the membrane potentials are more broadly tuned to a feature of interest than spikes of the same neuron (Bringuier et al. 1999; Zhu and Connors 1999; Carandini and Ferster 2000; Jia et al. 2010). Therefore, LFPs, if closely tracking the subthreshold membrane potentials, would be more broadly tuned than spikes. Second, the membrane potentials of the nearby neurons are highly correlated with one another even if their spikes are not correlated (LampI et al. 1999; Poulet and Petersen 2008). The high correlation of the membrane potentials among neighboring neurons is likely due to shared synaptic inputs (Shadlen and Newsome 1998), while the uncorrelated spikes may be explained by nonlinear transformations that are sensitive to small specific differences in the excitatory synaptic inputs between neurons (Poo and Isaacson 2009; Yu et al. 2009; Renart et al. 2010). In addition, averaging membrane potentials across many neurons will further smear the LFP sensitivity (Xing et al. 2009).

Because of these distinctive signal origins, LFPs may not change significantly while the spiking activity varies in the feature or cortical space. Conversely, significantly different LFPs can be observed without a significant change in the spiking activity. For example, perceptual changes were reflected in the low frequency LFPs but not in the spiking activity in the primary visual cortex (Gail et al. 2004; Wilke et al. 2006). As such, various kinds of LFP-spike relationship have been found across different species, brain areas, task conditions, and features of interest, suggesting that relationship between the two signals is highly specific to the functional connectivity of a local network (Liu and Newsome 2006; Kayser et al. 2007; Nir et al. 2007; Berens et al. 2008).

The high dependence of LFP-spike relationships on local connectivity predicts that a diversity in the relationships may exist even within one brain area under the same task condition if neurons in the area have heterogeneous input connectivity. PRR is a uniquely suited neural substrate to test this prediction

Address for reprint requests and other correspondence: E. J. Hwang, Division of Biology, Mail Code 216-76, California Institute of Technology, Pasadena, CA 91125 (e-mail: eunjung@caltech.edu).

for the following reasons. First, the region receives two distinct cortico-cortical inputs, bottom-up visual input from V6 and top-down motor input from dorsal premotor cortex (Johnson et al. 1996; Galletti et al. 2001). Second, PRR includes two classes of motor goal planning neurons differing in their connectivity to the two inputs; one class (visuomotor) appears to connect to the visual input more strongly than the other class (motor) (Gail and Andersen 2006; Hwang and Andersen 2008). Such input connectivity predicts that visual stimulation would affect the spike activity of the visuomotor neurons and the LFPs but not the spike activity of the motor neurons. Therefore, the LFP-spike relationships would be different between the two PRR neuronal classes in the presence of a visual stimulation.

To test this specific prediction, we examined how active visual inputs to PRR affect LFP-spike relations by comparing the delay period activity between two task conditions: visually guided vs. memory-guided reach. A visual stimulus at the reach target (goal) continued to be present during the delay period only in the visually guided reach task, allowing us to infer effects of the visual stimulus by computing differences in the delay period activity between the memory and visually guided reach tasks (Fig. 1, A and B). First, the visual stimulation increased the LFP power in the gamma bands, whether or not it increased the firing rate of the concurrently recorded neurons. Second, we classified neurons visuomotor if the visual stimulation increased their firing rates and the rest motor. Then, we compared the LFP-spike correlations between the two

neuronal classes within each task and found that the LFP-spike correlation was higher for the visuomotor neurons than the motor neurons in the visually guided reach, consistent with our prediction.

METHODS

Two male rhesus monkeys (*Macaca Mulatta*, *monkeys Y and G*) participated in this study. All procedures followed National Institutes of Health Guidelines and were approved by the California Institute of Technology Animal Care and Use Committee.

Memory-guided vs. visually guided reach tasks. The memory-guided reach trial began as the monkeys acquired the ocular and manual fixations in the screen center (memory-guided reach task; Fig. 1A). After a 0.5-s fixation period, a single reach target (green circle) appeared at a peripheral location for 0.3 s. The monkeys maintained the central fixation for a variable delay (1.3 ± 0.08 s) until the manual fixation target disappeared. Then, they reached to the remembered location without moving gaze from the fixation point. The reaction time from fixation target offset to reach onset was 0.27 ± 0.092 s for *monkey Y* and 0.42 ± 0.183 s for *monkey G*. After holding the hand on the reach target and maintaining eyes on the fixation target for 0.3 s, the monkeys received a juice reward. The visually guided reach trial was the same except that the reach target remained illuminated during the delay period (visually guided reach task; Fig. 1E). The reaction time in the visually guided reach was 0.28 ± 0.107 s for *monkey Y* and 0.41 ± 0.219 s for *monkey G*. The neural data analysis included only successful trials. Six targets evenly spaced around a virtual circle ($\sim 10.3^\circ$ eccentricity), and the two task conditions were pseudoran-

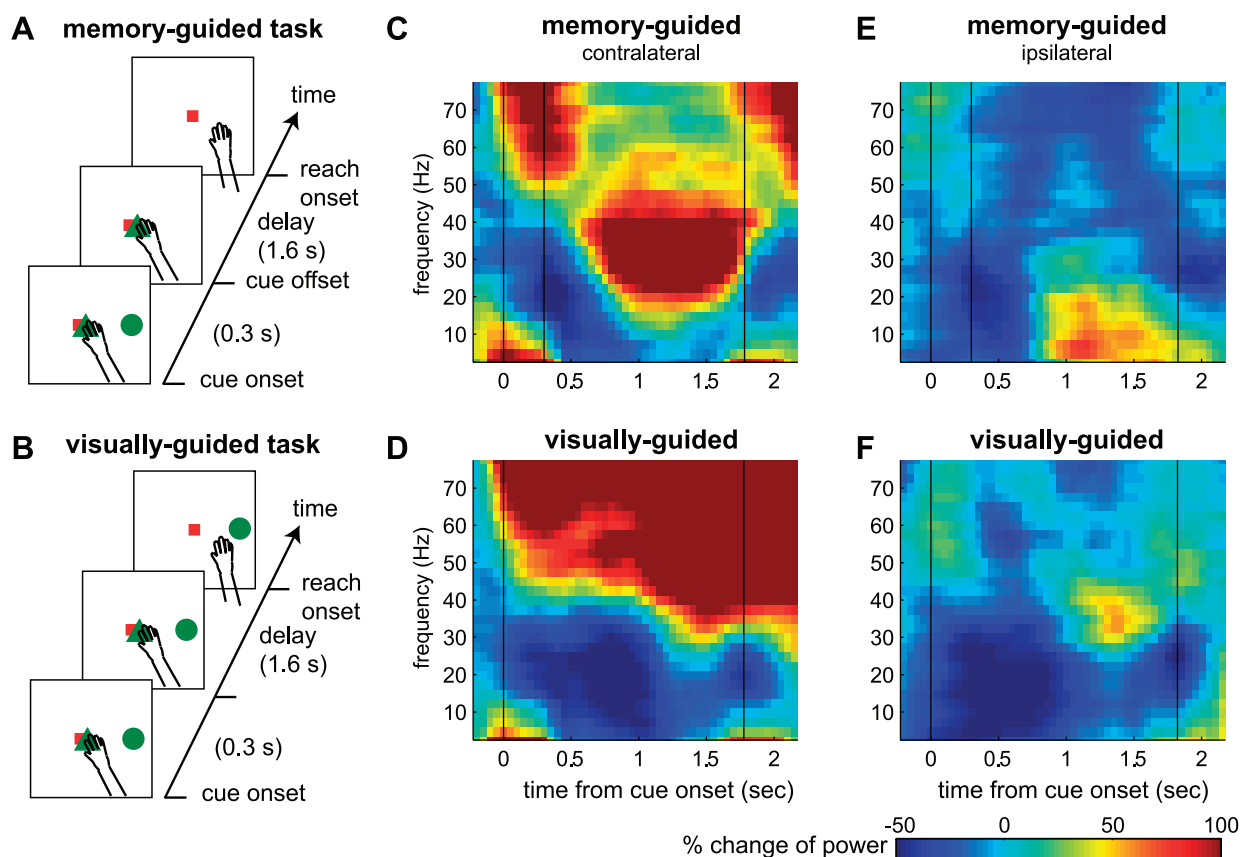


Fig. 1. Task sequence and local field potential (LFP) power spectrograms of an example site. A and B: event sequence of the memory-guided (visually guided) reach task. C and D: average power spectrogram for a reach goal on the contralateral side during the memory-guided (visually guided) reach task. E and F: same LFP site spectrogram for an ipsilateral side goal during the memory-guided (visually guided) reach task.

domly interleaved. In a complete recording session, the monkeys made at least 10 successful trials per target and task condition.

Extracellular recording. Both monkeys were implanted with a head holder and a recording chamber housing a 16-channel chronic microdrive (Neuralynx, Bowersman, MT) following the procedures described by Hwang and Andersen (2009). With the use of a commercial recording system (Plexon MAP System), neural activity from each electrode was amplified, filtered (LFP: 3.3–88 Hz and spike: 154 Hz–8.8 kHz), digitized (LFP: sampling rate 1 kHz and spike: 40 KHz), and then saved for further offline analysis. Previous studies (Pesaran et al. 2002; Scherberger et al. 2005) in our laboratory found that the cognitive state or reach goal information encoded in LFPs during the delay period is concentrated below ~ 90 Hz. Accordingly, we used a preamplifier with a built-in hardware band-pass filters passing the LFP signal < 88 Hz.

The recording chamber placement was guided and confirmed by structural magnetic resonance imaging, and recording was confined within the functionally premapped PRR area in the chamber. We further restricted our analysis to recording sites with neurons that satisfied the following criteria: 1) signal-to-noise ratio (the average trough-to-peak amplitude divided by twice the SD of spike wave forms) exceeds 3.5, and 2) the firing rate during the delay period is tuned to the reach goal in the memory-guided reach ($P < 0.05$, ANOVA with reach goal as a factor). One-hundred fifty-seven neurons (80 from *monkey Y*; 77 from *monkey G*) from 138 sites satisfied these criteria when the monkeys performed both the memory-guided and visually guided reach tasks. Unless explicitly stated otherwise, we combined data from both monkeys because they are qualitatively identical for our major findings.

Normalized LFP spectrogram. The raw LFP trace from each trial was transformed to a power spectrogram by computing a sequence of spectra over the 200-ms windows sliding with 50-ms steps, using multitaper methods with a 10-Hz bandwidth (Pesaran et al. 2002). The baseline power for each frequency was computed from the mean spectrum in the baseline period, averaged across all trials. The baseline period was a 0.2-s interval preceding cue onset. The spectrogram of each trial was normalized to the percent change from the baseline spectrum. That is, the change from the baseline power was divided by the baseline power.

Population average LFP spectrum. The population average LFP spectrum was computed separately for the contralateral and ipsilateral hemifields to the recording hemisphere because of the broad spatial tuning of LFPs with strong laterality. For example, the delay period LFP spectra for individual LFP sites were computed using all trials with reach goals on the contralateral side and then averaged across all sites to obtain the population average for the contralateral side. This data process provides a compact way to illustrate the difference in both the power and tuning of LFPs between the two tasks.

Frequency bands. To examine frequency band specific characteristics, we divided the frequency into eight bands (0–10, 10–20, . . . 70–80 Hz) and computed the average value in each frequency band. The significance level was adjusted using the Bonferroni correction (e.g., $P < 0.01/8$) when performing multiple comparisons in the eight frequency bands. We also examined the LFPs with a finer division of the low frequency bands into the conventional EEG bands, i.e., the delta (< 4 Hz), theta (4–8 Hz), alpha (8–12 Hz), and beta (~ 12 –30 Hz) bands and found that all EEG bands showed consistent trends with the 10-Hz step analysis (see Supplemental Fig. S3; Supplemental Material for this article is available online at the *J Neurophysiol* website).

Tuning strength and preferred direction. For any neural signal, including the spike firing rate and LFP power in each frequency band, the delay period was defined as the 1-s interval ending 0.2 s before reach onset. Within this interval, the visual stimulus at the reach goal was not present in the memory-guided reach task. The delay period activity of each signal from each task condition (10 trials/reach goal \times 6 reach goals) was subjected to a one-way ANOVA test with the reach

goal as a factor. If the tuning strength met the criteria $P < 0.05$, we considered the neural signal to be significantly tuned and computed its preferred direction.

The preferred direction was determined as the direction of a directional tuning vector (DTV) computed as follows: $DTV = \sum_{i=1}^6 r_i \vec{u}_i$, where r_i is the mean signal value for the i -th target and \vec{u}_i is the unit vector pointing to the i -th target (Gail and Andersen 2006). The circular variance (CV) has been shown to quantify the strength of circular tuning functions in other brain areas (Gur et al. 2005). Therefore, we computed the strength of a spatial tuning using CV as follows:

$$\text{tuning strength} = 1 - CV = \frac{\left| \sum_{i=1}^6 r_i \vec{u}_i \right|}{\sum_{i=1}^6 r_i}$$

Normalized spike density histogram. The raw spike trains of individual trials were convolved with a 200-ms rectangular window and averaged across trials. The average spike density histogram was normalized by 1) subtracting the baseline spike density, and then 2) dividing the amplitude by the mean delay period spike density for the preferred target in the memory-guided reach task.

Correlation between LFP power and firing rate. To examine the correlation in trial-by-trial fluctuations between the spiking and LFP activity recorded from the same electrode, we computed the Pearson's correlation coefficient between the LFP power in each frequency band and the firing rate over the 200-ms windows whose centers moved in 50-ms steps. The correlation coefficient was computed across all 60 trials in each task condition. The delay period correlation was computed by averaging the correlation coefficients within the 1-s interval ending 0.2 s before reach onset. Note that the correlation coefficients presented in this study were transformed from the Pearson's correlation coefficient to Fisher's z -score to conform to the assumption of a normal distribution.

RESULTS

We first examined effects of visual stimulation on LFPs in PRR by comparing the LFPs under the two task conditions: visually guided vs. memory-guided reach (Fig. 1, *A* and *B*). The most striking difference in LFPs between the two conditions was the power in the gamma range (> 40 Hz). Figure 1, *C* and *D*, shows power spectrograms of single site LFPs recorded for a reach goal on the contralateral side under the two conditions. In the memory-guided reach, the power in 20–40 Hz was the most strongly enhanced during the delay period, while the power in the gamma range became suppressed following the cue offset (Fig. 1*C*). In contrast, in the visually guided reach, the power in the gamma range was more sustained and stronger (Fig. 1*D*). Figure 1, *E* and *F*, shows the LFP power spectrograms of the same site for a reach goal on the ipsilateral side. Although the gamma range power for ipsilateral goals was much weaker than for the contralateral goals in both conditions, it was still stronger in the visually guided reach than the memory-guided reach. We confirmed that the LFP power in the gamma range was higher in the visually guided reach than the memory-guided reach at the population level (138 LFP sites). Figure 2, *A* and *B*, displays the population average of LFP power spectra during the delay period (1-s interval ending 0.2 s before reach onset) for both conditions and their difference. The LFP power in the gamma range frequency bands was significantly higher in the visually guided reach than the memory-guided reach for both contralateral and ipsilateral sides, albeit less strongly for ipsilateral side.

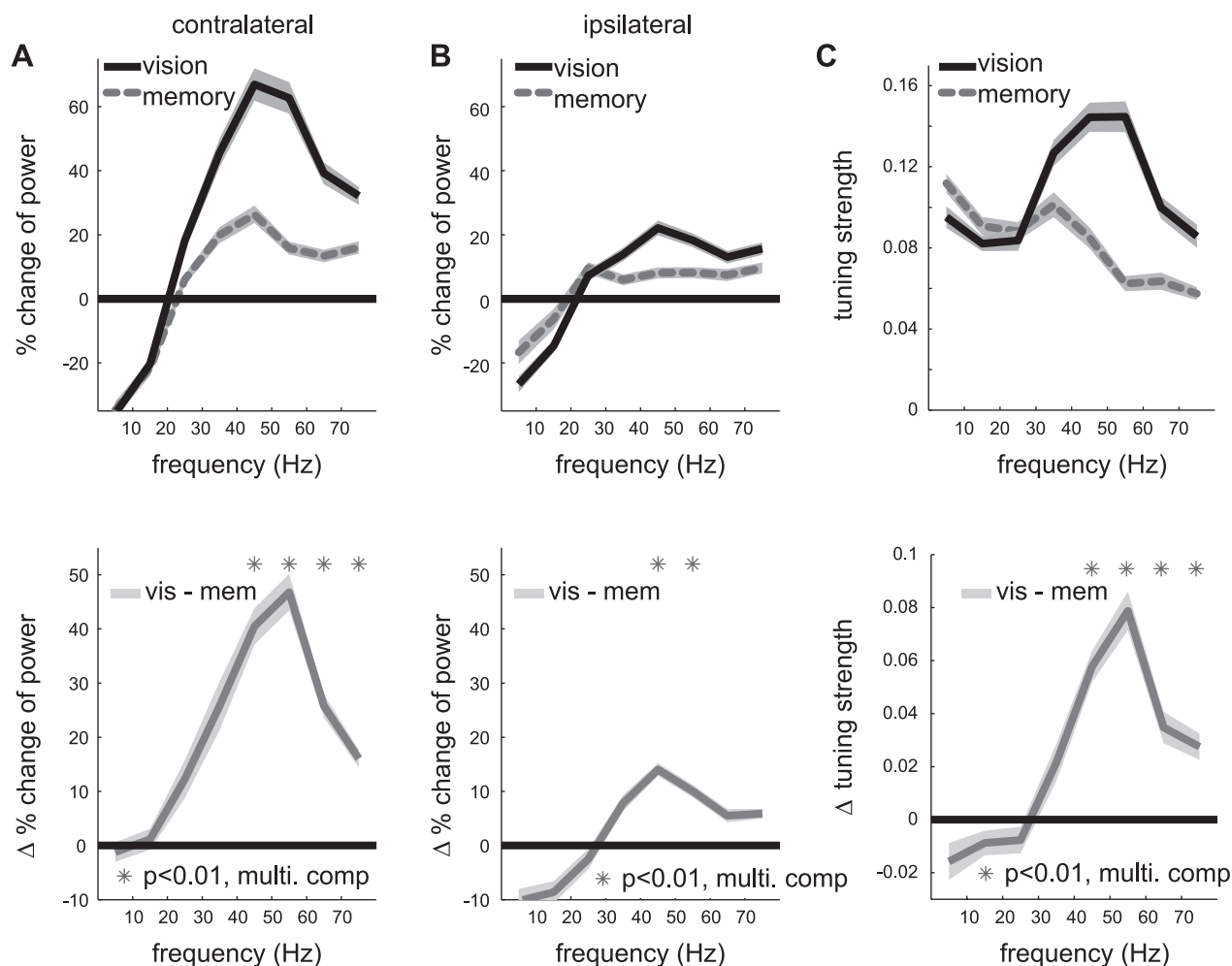


Fig. 2. Difference in the LFP power and spatial tuning strength between the 2 tasks. *A*, top: average LFP power spectra during the delay period for the contralateral side targets in the 2 reach tasks ($n = 138$); bottom: difference in the LFP power spectra between the 2 conditions. *B*: same as *A* but for the average power for ipsilateral side targets. *C*: similar to *A* but for the spatial tuning strength (1-circular variance). In all plots, line and bands represent the means \pm SE across the population, respectively.

In contrast to the gamma bands, intertask LFP power differences in the lower frequency bands (<40 Hz) were inconsistent between the two monkeys as shown in Fig. 3. For *monkey G*, the lower frequency power was higher in the visually guided reach than the memory-guided reach. For *monkey Y*, the opposite was observed. Consequentially, the mean power decrease <20 Hz for the ipsilateral side was significant for only one subject (refer to Supplementary Material for further discussion).

As shown in the single site spectrograms and the population average spectra, the LFP power was spatially tuned. We examined how the strength of spatial tuning was affected by visual stimulation. Because the power enhancement was stronger for the contralateral side, the spatial tuning was significantly strengthened in the gamma bands in the visually guided reach (Fig. 2C). Therefore, the increased power in the gamma bands encodes spatial information of the visual stimulus and thus is not a mere global signal indicating a simple context difference between the two conditions, i.e., the absence vs. the presence of a visual stimulus.

For those LFP sites that showed significant spatial tuning during the delay period, we computed the preferred direction (see METHODS). Figure 4 shows the distribution of the preferred

directions for each frequency band under each condition. In general, the preferred direction rotated from the ipsilateral side to the contralateral side as the frequency increases, especially in the memory-guided reach. To see if this rotation occurs within each LFP site, we examined the preferred directions of LFP sites that were significantly tuned in both lower and higher frequency bands. As Table 1 shows, LFP sites tuned in both frequency bands tend to have their preferred direction on the ipsilateral side for the lower frequency bands but contralateral side for the higher frequency bands under both conditions. In addition, trial-by-trial fluctuations of the power in the low frequency bands (<20 Hz) and the power in the higher frequency bands (>40 Hz) within individual sites tended to covary in an anticorrelated manner during the delay period (Supplemental Fig. S2). These results confirm that the rotation occurred within LFP sites and reject the possibility that the two tasks recruited two separate populations of LFP sites, each with different preferred directions.

It may also appear that the preferred direction in the gamma bands rotated slightly towards the lower contralateral visual field in the visually guided reach relative to the memory-guided reach. However, this rotation did not occur within individual sites that were tuned in both conditions. Instead, this apparent

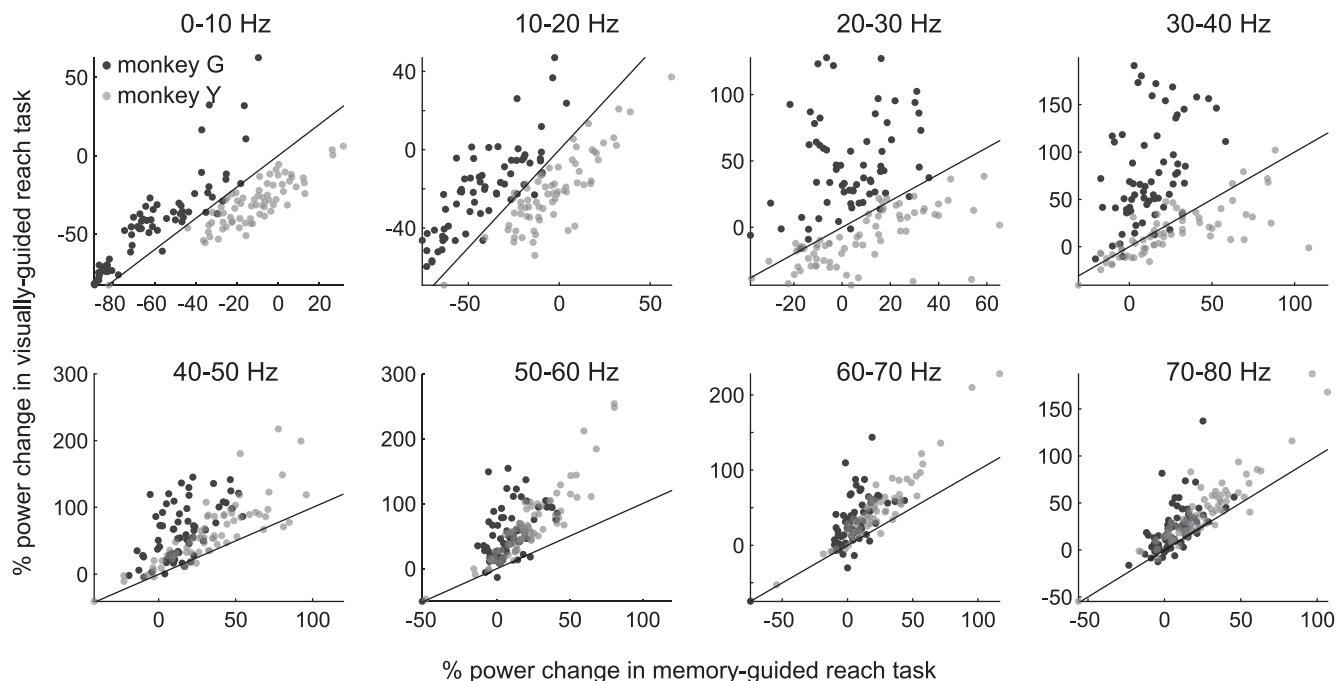


Fig. 3. LFP power in the memory-guided vs. in the visually guided reach task in each frequency band for 2 monkeys. Each dot represents a single LFP site. Black lines are unity lines.

rotation emerged because the LFP sites which were not tuned in the memory-guided condition became tuned in the visually guided condition with a preferred direction mostly toward the lower contralateral side. For instance, 52 LFP sites were not tuned in the memory-guided reach and became significantly tuned in the visually guided reach in the 40- to 50-Hz band. Forty-two of these fifty-two sites had their preferred direction in the lower contralateral side. The ratio was 53/71, 46/58, and 26/37 in the 50–60, 60–70, and 70–80 Hz bands, respectively.

Next, we examined the spiking activity of the neurons that were simultaneously recorded on the same electrode as the LFPs. If a neuron receives strong visual input, it would be elicited by visual stimuli, leading to more active response during the delay period in the visually guided reach compared with the memory-guided reach. For example, Fig. 5A shows the firing response of a neuron recorded from the same electrode as the LFPs shown in Fig. 1. This neuron showed a stronger delay period response before reaches to the preferred

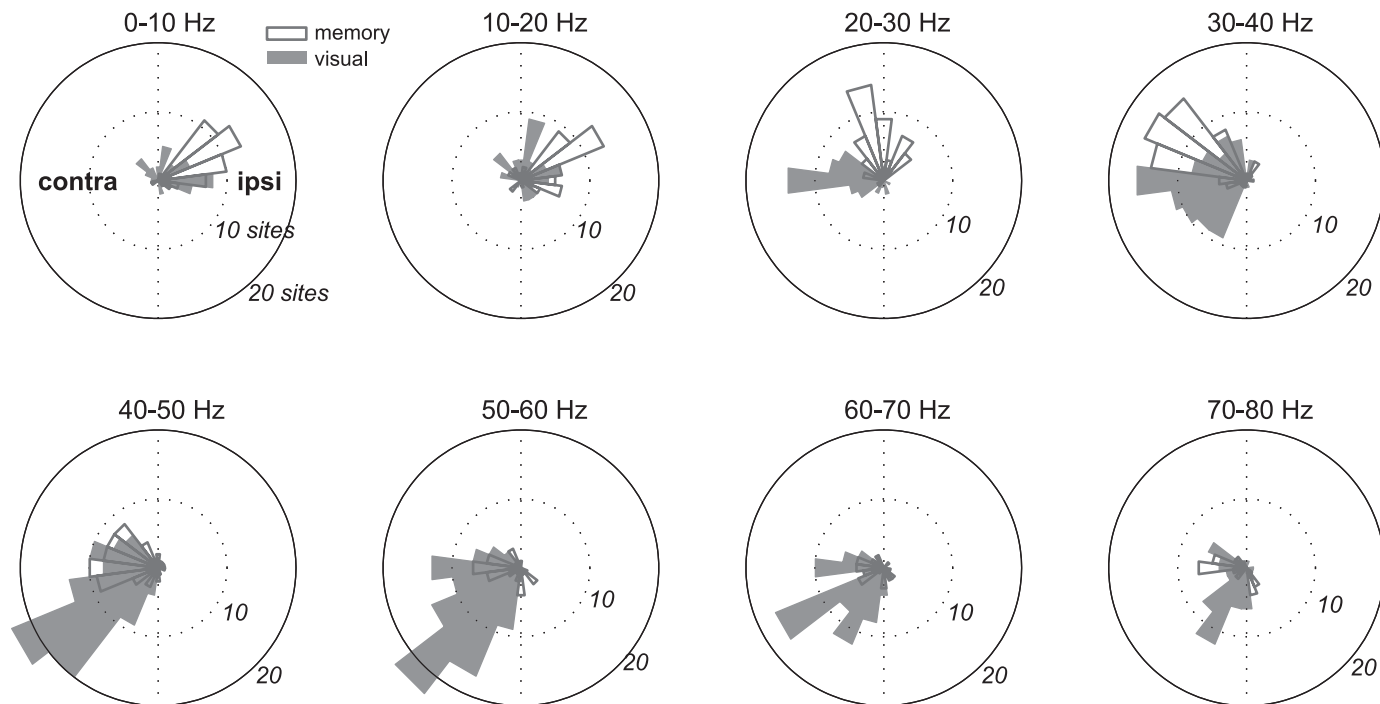


Fig. 4. Distributions of the preferred directions of the delay period LFP power in 8 frequency bands for the 2 task conditions.

Table 1. LFP sites tuned in both frequency bands

	0–10/10–20, Hz	0–10/20–30, Hz	0–10/30–40, Hz	0–10/40–50, Hz	10–20/20–30, Hz	10–20/30–40, Hz	10–20/40–50, Hz	10–20/50–60, Hz
Contra/Ipsi	0 (0)	0 (1)	0 (0)	0 (0)	0 (1)	0 (0)	0 (0)	0 (1)
Ipsi/Ipsi	27 (17)	5 (1)	1 (1)	3 (0)	7 (3)	1 (2)	4 (0)	4 (0)
Contra/Contra	2 (6)	1 (8)	1 (9)	2 (8)	5 (10)	5 (12)	4 (12)	2 (11)
Ipsi/Contra	0 (2)	11 (8)	24 (20)*	27 (28)*	9 (9)	23 (18)*	26 (31)*	12 (34)*

Local field potentials (LFP) sites that were significantly tuned in both at a low frequency band and a higher frequency band were divided into 4 different combinations of laterality of preferred directions for each of 8 paired frequency bands. For example, the first column shows the number of LFP sites that had the preferred direction on the contralateral side in a 0- to 10-Hz frequency band and the ipsilateral side in a 10- to 20-Hz frequency band. Numbers outside parenthesis are for the memory-guided reach, while the numbers inside parenthesis are for the visually guided reach. *Ipsi/Contra was the majority in both subjects.

target in the visually guided reach than the memory-guided reach. In contrast, the example neuron in Fig. 5B showed no difference in the delay period response between the two tasks. We compared the delay period firing rate between the two reach tasks for individual neurons (Fig. 6A) and found that a subpopulation of neurons indeed showed higher firing rate in the visually guided reach than the memory-guided reach. If neurons fired more during the visually guided reach than the memory-guided reach by three or more spikes per second, they were classified as visuomotor. Otherwise, neurons were clas-

sified as motor. This threshold (3 spikes) corresponds to the midpoint between the two prominent peaks in the distribution of the intertask differences in the firing rate (Fig. 6B). For this threshold, 32% of neurons were visuomotor and their firing rate in the visually guided reach was higher than the memory-guided reach by 11 ± 9.1 spikes for the preferred target [$P < 1e-10$, paired t -test; $t_{(49)} = 8.6$]. Of course, proportions of the two classes depend on the threshold value, but the results described hereafter statistically holds true for a range of thresholds, 0–9. It is also noteworthy that when the neurons were

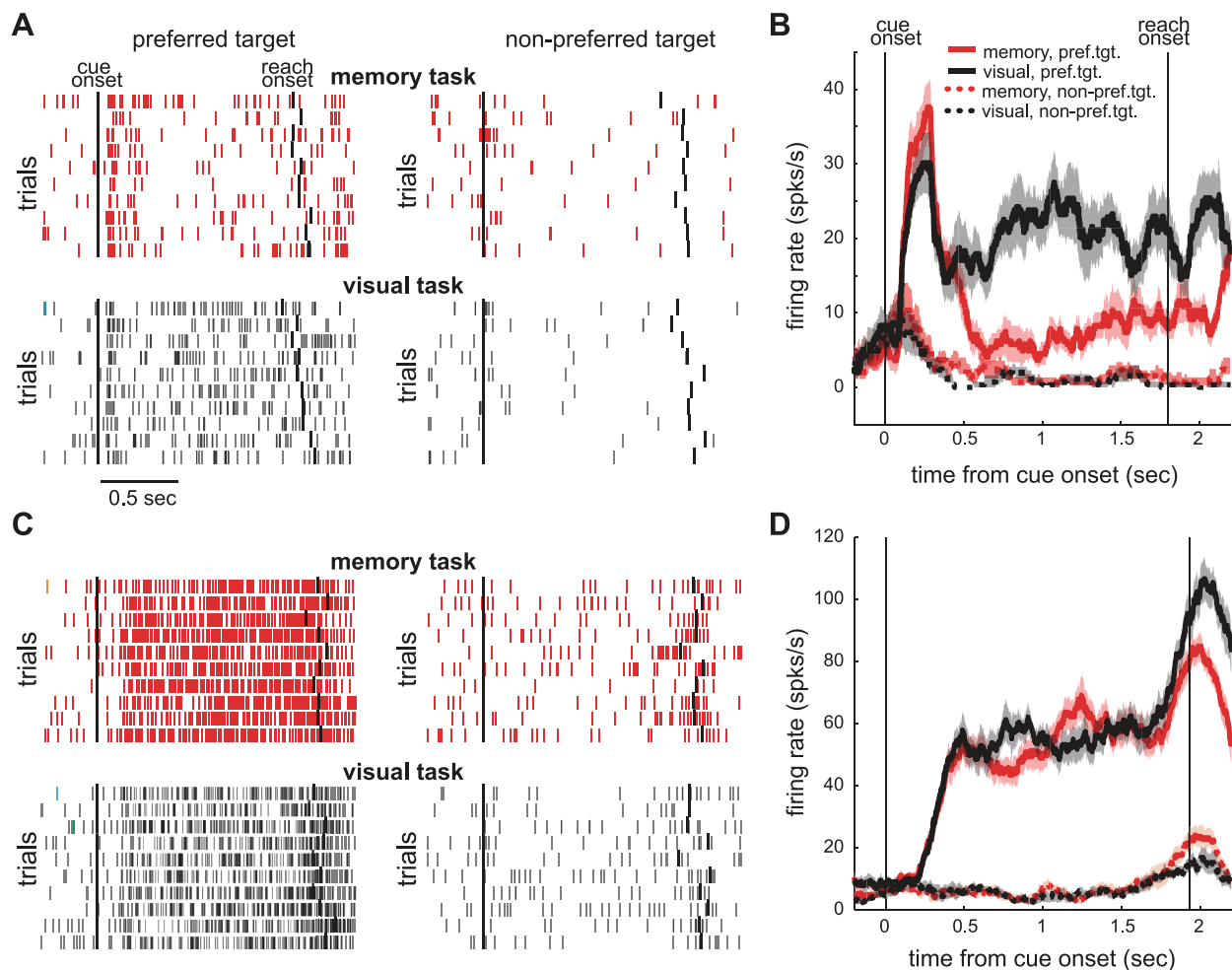


Fig. 5. Two example neurons. *A*: spike rasters of a neuron that was recorded from the same electrode as the LFPs shown in Fig. 1. Ten trials for each of its preferred and nonpreferred reach targets. Preferred target was the same between the 2 tasks and was on the contralateral to the recording hemisphere. Nonpreferred target was 180° rotated from the preferred target. For each trial, the black thick bars indicate cue onset and reach onset from left to right. *B*: spike density histogram (means \pm SE) of the neuron in *A*. Vertical lines indicate the cue onset and the average reach onset. *C* and *D*: same as *A* and *B* but for another example neuron.

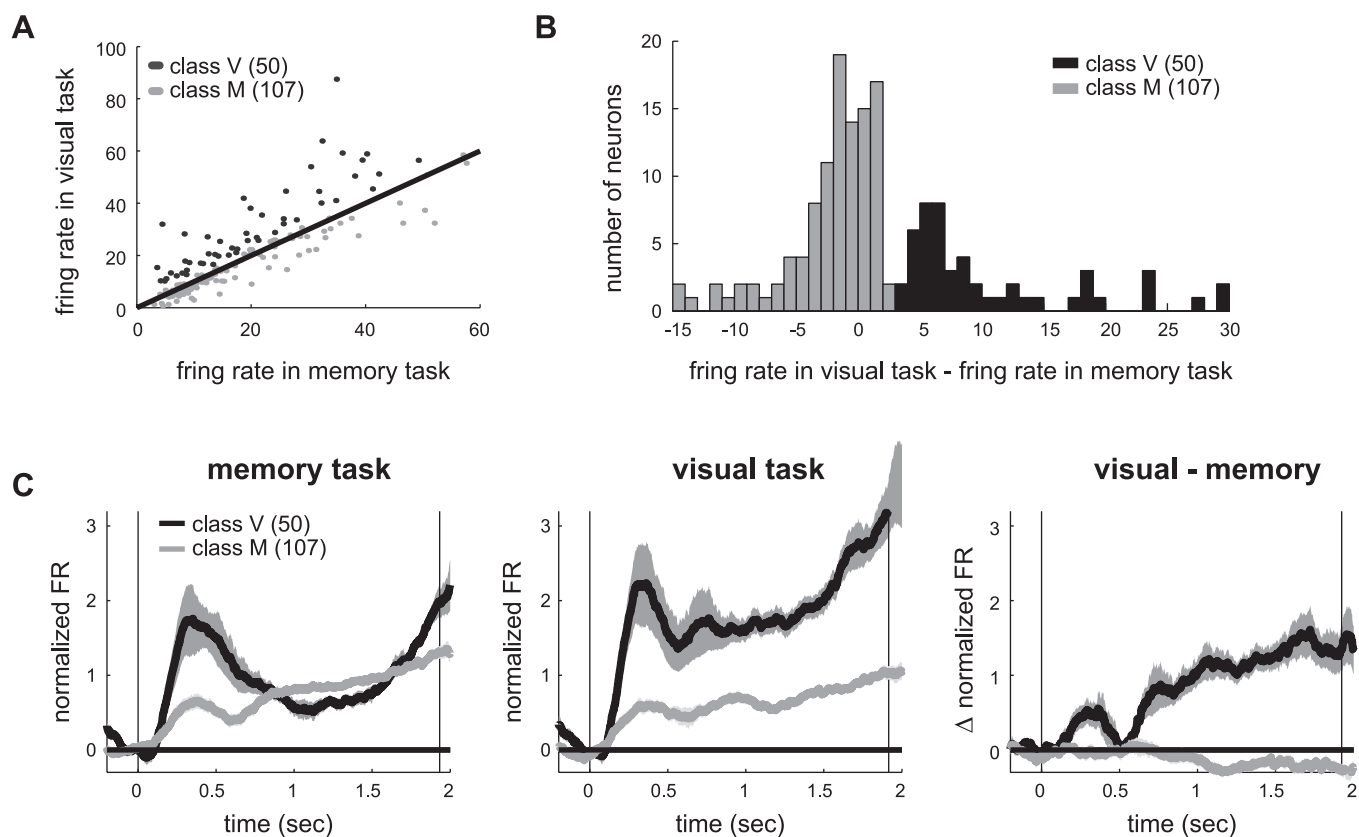


Fig. 6. Two neuronal classes. *A*: delay period firing rate in the memory-guided reach vs. visually guided reach. Each dot corresponds to a single neuron. Solid line is the unity line. *B*: distribution of the difference in the delay period firing rates between the 2 task conditions. *C*: average spike density histograms for the preferred target for 2 classes of neurons. *Left*: memory-guided reach; *middle*: visually guided reach; *right*: difference between the 2 reach tasks.

classified into three classes instead of two so that one class had a stronger response in the visually guided reach, another had a stronger response in the memory-guided reach, and the last had similar responses in the two tasks, comparisons between the former two classes produced essentially the same results as comparisons between the visuomotor and motor neuron classes reported hereafter (Supplemental Fig. S5).

Figure 6C displays the mean temporal dynamics of the firing rate separately for the two classes and the two tasks. Congruent with the different response sensitivity to the visual stimulation during the delay period, the visuomotor neurons showed strong transient visual response upon the stimulus onset, which was absent in the motor neurons. One may wonder if the LFPs recorded with the above neurons varied with the neuronal class. However, it is unlikely because 6 of 17 neuronal pairs that were simultaneously recorded from the same electrode were classified as belonging to different classes, suggesting that the two classes were anatomically intermingled (see Supplemental Fig. S4 for an example pair). Indeed, Fig. 7A shows the LFP power spectra during the delay period averaged across all recording sites of each class separately. Unlike the distinct spike firing patterns, the LFP power spectra were similar between the two classes under both conditions and thus in their differences between the conditions. Similar to the power spectra, the LFP tuning strength was not different between the two classes, either (Fig. 7B). Thus the visual stimulus at the reach goal increased the LFP power in the gamma bands and strengthened their spatial tuning whether or not the simultaneously recorded spiking activity was also affected.

Finally, we tested our prediction that the LFP-spike relations would differ between the two classes of neurons in the presence of the visual stimulus. To do so, we measured the degree of correlation in trial-by-trial fluctuations between the LFP power and the firing rate of the neurons recorded on the same electrode (see METHODS). The correlations in the gamma bands were positive and indistinguishable between the two neuronal classes in the memory-guided reach in which the visual stimulus was absent (Fig. 7C). However, correlations in the gamma bands became significantly stronger for the visuomotor than motor neurons in the visually guided reach ($P < 0.01$, two-sample t -test). Thus the change in the correlation induced by the visual stimulation was significantly different in the gamma bands between the two subpopulations ($P < 0.01$, two-sample t -test). The interclass difference in correlation in the visually guided reach is not due to the sensitivity of the measure to the firing rate or LFP power per se for the following reasons: 1) when the neurons were divided into three different groups within each class based on their delay period firing rate in the visually guided reach task, the correlation for low firing rate neurons was not different from high firing rate neurons in any task or any class (Supplemental Fig. S6); and 2) the correlation measured for spike and LFPs recorded from different sites (random-pair) was significantly different from zero for the visuomotor neurons in the visually guided reach, but the random-pair correlations were significantly smaller than the true-pair correlations (Supplemental Fig. S7). If the visual stimulation causes the interclass difference in the LFP-spike relations, a similar difference should occur during the cue period of both tasks when

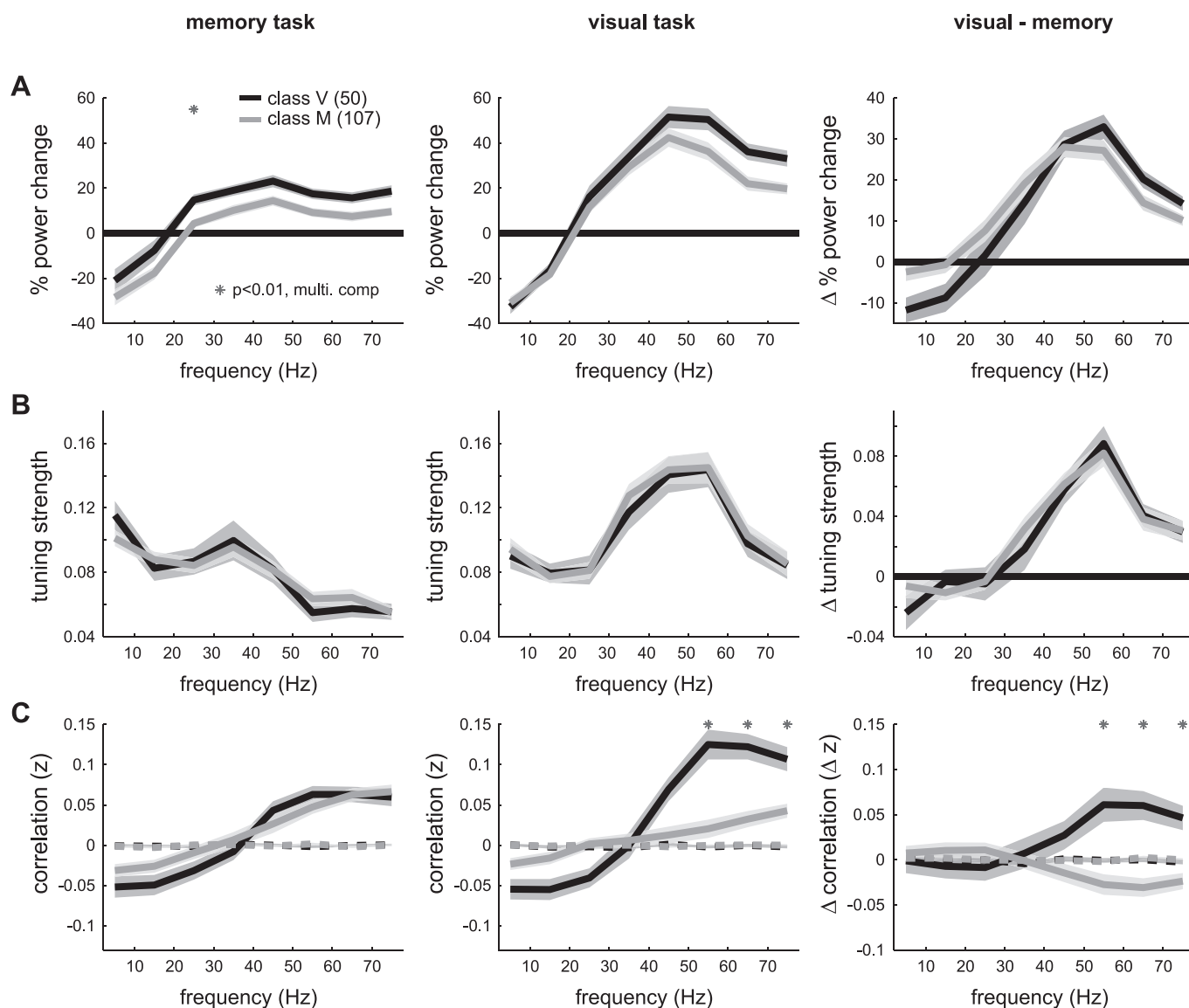


Fig. 7. Relationship between LFP power and firing rate depends on the neuronal class. *A*: average LFP power during the delay period. In all 3 rows: *left*: memory-guided reach; *middle*: visually guided reach; *right*: difference between the 2 reach tasks. *B*: average tuning strength. *C*: average correlation coefficient between the LFP power in each frequency band and the firing rate during the delay period. Dotted lines indicate the means \pm SE of the correlation for the trial shuffled LFPs and spikes in each condition.

the visual stimulation was present. Indeed, we found that the gamma LFP-spike correlation was stronger for the visuomotor neurons than the motor neurons during the cue period in both tasks (Supplemental Fig. S8). Taken together, in the presence of visual stimulus, the LFP gamma power was better correlated with the firing rate of the visuomotor neurons than the firing rate of the motor neurons, confirming our prediction.

DISCUSSION

In our study, we hypothesized that the LFP-spike relationship could vary even within one brain area under the same task condition if neurons in the area have heterogeneous connectivity with the input sources. We tested the hypothesis in PRR in which two classes of neurons showed different connectivity to the visual input by comparing the effects of visual stimulations on LFPs, spikes, and their

interrelations between the visuomotor and motor neurons. First, we confirmed the heterogeneous connectivity in PRR; the visual stimulation increased the firing rate for a subpopulation of neurons (visuomotor) but not for the other (motor). Second, the visual stimulation increased the LFP power in the gamma bands regardless of the class of the neurons. Third, the visual stimulation rendered the correlation between the LFP power and the firing rate stronger for the visuomotor neurons than for the motor neurons. These results support our hypothesis, indicating that LFPs vary with the stimulation condition and that the LFP-spike relationship depends on a given neuron's connectivity to the dominant input sources in a specific stimulation condition.

Relationship between LFP gamma oscillations and firing rate. The relationship between the gamma oscillations and firing rate vary widely among different brain areas and stimulation conditions (Liu and Newsome 2006; Kayser et al. 2007;

Nir et al. 2007; Berens et al. 2008). In our study, separate analyses for the two neuronal subpopulations enabled us to examine how the relationship between the gamma range LFPs and spikes varies depending on stimulation conditions and their connections to the stimulus input sources. For the same neurons, the correlation coefficient between the LFP power and the spike firing rate changed when the visual stimulation condition changed. The relationship also differed between the two subpopulations with different visual input connections under the same stimulation condition. What kind of functional connectivity explains such variable relationships in PRR?

Suppose that the gamma oscillations in the memory-guided reach task are weakly driven by common inputs that both classes of neurons share, e.g., local and top-down motor inputs, while the gamma oscillations in the visually guided reach task are strongly driven by the visual input in conjunction with the common inputs (Fig. 8). Then, the average correlation would be approximately equal for the two subpopulations in the memory-guided reach because they both receive the governing common inputs (Fig. 8A). In the visually guided reach, however, the average correlation for motor neurons would become lower because only the visuomotor neurons receive strong visual inputs (Fig. 8B). Therefore, an explanation of the wide variability in relationship between the gamma range LFPs and spikes may be that inputs governing the gamma oscillations are not unique, and they change with stimulus condition. Thus the correlation between a neuron's firing rate and the gamma oscillations would also change, depending on the neuron's connection strength with the gamma-governing inputs in each particular condition.

If the degree of overlap between the gamma-governing inputs and the excitatory inputs of a neuron underlies the observed variable correlations, a similar variability may manifest in spike-LFP coherence, i.e., degree of phase coherence between the two signals (Pesaran et al. 2002; Buschman and Miller 2007). In other words, the firing rate of the input neurons carrying the visual signal would be well synchronized with both the

gamma oscillations and the visuomotor neuron but not with the motor neurons. Consequently, the gamma oscillation would show higher coherence with the visuomotor neurons than the motor neurons in the presence of the visual stimulation. In fact, we observed this trend although the variability of the coherence estimate was rather large in part because of the insufficient number of trials (Supplemental Fig. S9).

Enhanced LFP gamma oscillations by visual stimulation. It is of interest to know whether the visual input by itself was a dominant driver relative to the other inputs that existed in the memory-guided reach or whether the visual input acted as a modulator to enhance the existing effect of the other inputs. Our experiments were not equipped to dissociate these two mechanisms because both the visual and the other inputs were available and carried congruous spatial information in our visually guided reach. A task in which the visual inputs during the delay period are spatially incongruent or uncorrelated with the reach goal may address this issue. If visual inputs by themselves are the dominant input driving gamma oscillations, the gamma oscillations would encode the location of the visual stimulus instead of the reach goal. Likewise if the visual inputs modulate the gamma oscillations that encode the motor input, the gamma oscillations would encode the reach goal. This issue will be particularly important when using LFPs in neural prosthetic applications in which the motor intention must be distinguished from visual distractors (Andersen and Cui 2009; Andersen et al. 2010).

Lower frequency oscillations. An intriguing finding from our study is that the preferred direction that elicited the highest LFP power rotated from ipsilateral to contralateral side as the frequency increases. Consistently, the trial-by-trial fluctuation of LFP power in response to the variation of the reach goal was anticorrelated between the lower (<20 Hz) and higher frequency (>40 Hz) bands in both monkeys (Supplemental Fig. S2). The anticorrelated or uncorrelated power change between the lower

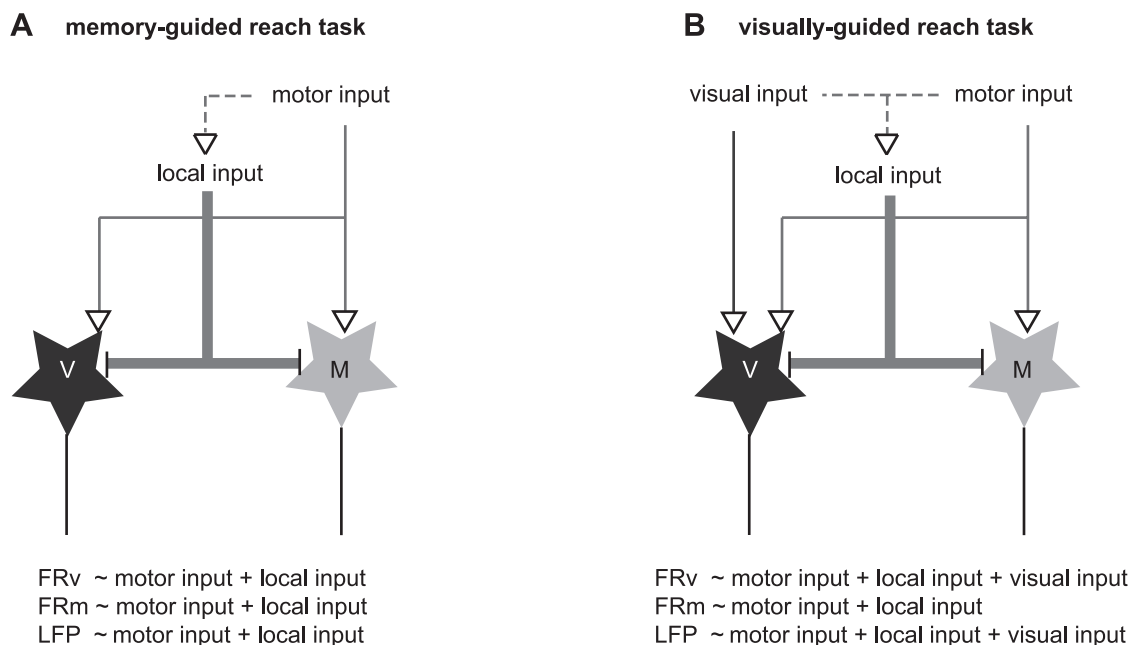


Fig. 8. Schematic diagrams of the network connectivity in the 2 task conditions. Black stars represent the visuomotor neurons, while the grey stars represent the motor neurons. Equations indicate the relationship between the firing rates of each class of neurons or LFPs and the input sources in each task condition.

and higher frequency bands has been reported in other studies as well (Fries et al. 2001; Rickert et al. 2005; Asher et al. 2007; Nir et al. 2007; Belitski et al. 2008; Hwang and Andersen 2009). If the complementary changes in the low and high frequency bands are an intrinsic property of LFPs, this trend would show in spontaneous activity as well. Rejecting this possibility, the correlation during the fixation period (0.5-s interval before stimulus onset) was uncorrelated or slightly positively correlated (data now shown). Alternatively, the anticorrelated tuning during the delay period may arise if two separate input sources that are anticorrelated drive the oscillations in the two frequency bands. A possible input source for the low frequency oscillations in PRR is the ipsilateral hemisphere, albeit much weaker than the contralateral input (Kagan et al. 2010). If the ipsilateral input drives oscillations, the oscillation frequency is likely to be lower than the contralateral input in order to be robust to the spike timing delays, which may be achieved by the larger conduction delay itself or through synapses with slower membrane time constants than the contralateral input (Whittington et al. 1995; Engel et al. 2001).

ACKNOWLEDGMENTS

We thank Chess Stetson and Drs. Igor Kagan, Melanie Wilke, and Alexander Gail for scientific discussion; Tessa Yao for editorial assistance; Kelsie Pejisa and Nicole Simmons for animal care; and Viktor Shcherbatyuk for technical assistance.

GRANTS

This work was supported by National Eye Institute Grant EY-013337. E. J. Hwang was supported by NIH Research Service Award T32 NS007251 and Career Development Award K99 NS062894.

DISCLOSURES

No conflicts of interest, financial or otherwise, are declared by the author(s).

REFERENCES

- Andersen RA, Cui H. Intention, action planning, and decision making in parietal-frontal circuits. *Neuron* 63: 568–583, 2009.
- Andersen RA, Hwang EJ, Mulliken GH. Cognitive neural prosthetics. *Annu Rev Psychol* 61: –190, C161–163, 2010.
- Asher I, Stark E, Abeles M, Prut Y. Comparison of direction, and object selectivity of local field potentials and single units in macaque posterior parietal cortex during prehension. *J Neurophysiol* 97: 3684–3695, 2007.
- Axel F, Reinhard E. Functional coupling shows stronger stimulus dependency for fast oscillations than for low-frequency components in striate cortex of awake monkey. *Eur J Neurosci* 12: 1466–1478, 2000.
- Belitski A, Gretton A, Magri C, Murayama Y, Montemurro MA, Logothetis NK, Panzeri S. Low-frequency local field potentials and spikes in primary visual cortex convey independent visual information. *J Neurosci* 28: 5696–5709, 2008.
- Berens P, Keliris GA, Ecker AS, Logothetis NK, Tolias AS. Comparing the feature selectivity of the gamma-band of the local field potential and the underlying spiking activity in primate visual cortex. *Front Syst Neurosci* 2: 2, 2008.
- Bringuier V, Chavane F, Glaeser L, Frégnac Y. Horizontal propagation of visual activity in the synaptic integration field of area 17 neurons. *Science* 283: 695–699, 1999.
- Buschman TJ, Miller EK. Top-down versus bottom-up control of attention in the prefrontal and posterior parietal cortices. *Science* 315: 1860–1862, 2007.
- Carandini M, Ferster D. Membrane potential and firing rate in cat primary visual cortex. *J Neurosci* 20: 470–484, 2000.
- Engel AK, Fries P, Singer W. Dynamic predictions: oscillations and synchrony in top-down processing. *Nat Rev Neurosci* 2: 704–716, 2001.
- Fries P, Reynolds JH, Rorie AE, Desimone R. Modulation of oscillatory neuronal synchronization by selective visual attention. *Science* 291: 1560–1563, 2001.
- Gail A, Andersen RA. Neural dynamics in monkey parietal reach region reflect context-specific sensorimotor transformations. *J Neurosci* 26: 9376–9384, 2006.
- Gail A, Brinkmeyer HJ, Eckhorn R. Perception-related modulations of local field potential power and coherence in primary visual cortex of awake monkey during binocular rivalry. *Cereb Cortex* 14: 300–313, 2004.
- Galletti C, Gamberini M, Kutz D, Fattori P, Luppino G, Matelli M. The cortical connections of area V6: an occipito-parietal network processing visual information. *Eur J Neurosci* 13: 1572–1588, 2001.
- Gray CM, Singer W. Stimulus-specific neuronal oscillations in orientation columns of cat visual cortex. *Proc Natl Acad Sci USA* 86: 1698–1702, 1989.
- Gur M, Kagan I, Snodderly DM. Orientation, and direction selectivity of neurons in V1 of alert monkeys: functional relationships and laminar distributions. *Cereb Cortex* 15: 1207–1221, 2005.
- Heldman DA, Wang W, Chan SS, Moran DW. Local field potential spectral tuning in motor cortex during reaching. *IEEE Trans Neural Syst Rehabil Eng* 14: 180–183, 2006.
- Henrie JA, Shapley R. LFP power spectra in V1 cortex: the graded effect of stimulus contrast. *J Neurophysiol* 94: 479–490, 2005.
- Hwang EJ, Andersen RA. The parietal reach region represents the spatial goal in symbolically instructed reaches. In: *Society for Neuroscience*. Washington DC: 2008 Neuroscience Meeting Planner, 2008.
- Hwang EJ, Andersen RA. Brain control of movement execution onset using local field potentials in posterior parietal cortex. *J Neurosci* 29: 14363–14370, 2009.
- Jia H, Rochefort NL, Chen X, Konnerth A. Dendritic organization of sensory input to cortical neurons in vivo. *Nature* 464: 1307–1312, 2010.
- Johnson PB, Ferraina S, Bianchi L, Caminiti R. Cortical networks for visual reaching: physiological, and anatomical organization of frontal and parietal lobe arm regions. *Cereb Cortex* 6: 102–119, 1996.
- Kagan I, Iyer A, Lindner A, Andersen RA. Space representation for eye movements is more contralateral in monkeys than in humans. *Proc Natl Acad Sci USA* 107: 7933–7938, 2010.
- Kayser C, Petkov CI, Logothetis NK. Tuning to sound frequency in auditory field potentials. *J Neurophysiol* 98: 1806–1809, 2007.
- Lamp I, Reichova I, Ferster D. Synchronous membrane potential fluctuations in neurons of the cat visual cortex. *Neuron* 22: 361–374, 1999.
- Leopold DA, Logothetis NK. Spatial patterns of spontaneous local field activity in the monkey visual cortex. *Rev Neurosci* 14: 195–205, 2003.
- Liu J, Newsome WT. Local field potential in cortical area MT: stimulus tuning and behavioral correlations. *J Neurosci* 26: 7779–7790, 2006.
- Nir Y, Fisch L, Mukamel R, Gelbard-Sagiv H, Arieli A, Fried I, Malach R. Coupling between neuronal firing rate, gamma LFP, and BOLD fMRI is related to interneuronal correlations. *Curr Biol* 17: 1275–1285, 2007.
- O’Leary JG, Hatsopoulos NG. Early visuomotor representations revealed from evoked local field potentials in motor and premotor cortical areas. *J Neurophysiol* 96: 1492–1506, 2006.
- Penttonen M, Kamondi A, Acsady L, Buzsaki G. Gamma frequency oscillation in the hippocampus of the rat: intracellular analysis in vivo. *Eur J Neurosci* 10: 718–728, 1998.
- Pesaran B, Pezaris JS, Sahani M, Mitra PP, Andersen RA. Temporal structure in neuronal activity during working memory in macaque parietal cortex. *Nat Neurosci* 5: 805–811, 2002.
- Poo C, Isaacson JS. Odor representations in olfactory cortex: “sparse” coding, global inhibition, and oscillations. *Neuron* 62: 850–861, 2009.
- Poulet JFA, Petersen CCH. Internal brain state regulates membrane potential synchrony in barrel cortex of behaving mice. *Nature* 454: 881–885, 2008.
- Renart A, de la Rocha J, Bartho P, Hollender L, Parga N, Reyes A, Harris KD. The asynchronous state in cortical circuits. *Science* 327: 587–590, 2010.
- Rickert J, Oliveira SC, Vaadia E, Aertsen A, Rotter S, Mehring C. Encoding of movement direction in different frequency ranges of motor cortical local field potentials. *J Neurosci* 25: 8815–8824, 2005.
- Scherberger H, Jarvis MR, Andersen RA. Cortical local field potential encodes movement intentions in the posterior parietal cortex. *Neuron* 46: 347–354, 2005.
- Shadlen MN, Newsome WT. The variable discharge of cortical neurons: implications for connectivity, computation, and information coding. *J Neurosci* 18: 3870–3896, 1998.
- Spinks RL, Kraskov A, Brochier T, Umiltà MA, Lemon RN. Selectivity for grasp in local field potential and single neuron activity recorded simultane-

- ously from M1 and F5 in the awake macaque monkey. *J Neurosci* 28: 10961–10971, 2008.
- Whittington MA, Traub RD, Jefferys JGR.** Synchronized oscillations in interneuron networks driven by metabotropic glutamate receptor activation. *Nature* 373: 612–615, 1995.
- Wilke M, Logothetis NK, Leopold DA.** Local field potential reflects perceptual suppression in monkey visual cortex. *Proc Natl Acad Sci USA* 103: 17507–17512, 2006.
- Xing D, Yeh CI, Shapley RM.** Spatial spread of the local field potential and its laminar variation in visual cortex. *J Neurosci* 29: 11540–11549, 2009.
- Yu YC, Bultje RS, Wang X, Shi SH.** Specific synapses develop preferentially among sister excitatory neurons in the neocortex. *Nature* 458: 501–504, 2009.
- Zhu JJ, Connors BW.** Intrinsic firing patterns and whisker-evoked synaptic responses of neurons in the rat barrel cortex. *J Neurophysiol* 81: 1171–1183, 1999.

